Chemical Physics Letters 605–606 (2014) 115–120

Contents lists available at ScienceDirect

Chemical Physics Letters

journal homepage: www.elsevier.com/locate/cplett

Square-centimeter-scale 2D-arrays of Au@Ag core–shell nanoparticles towards practical SERS substrates with enhancement factor of 10^7

Francesca Pincella [a,b,*], Yeji Song [a,b], Takao Ochiai [a,b], Katsuhiro Isozaki [c], Kenji Sakamoto [a], Kazushi Miki [a,b,*]

[a] Polymer Materials Unit, National Institute for Materials Science, 1-1 Namiki, Tsukuba, Ibaraki 305-0044, Japan
[b] Department of Pure and Applied Sciences, University of Tsukuba, 1-1-1 Tennodai, Tsukuba, Ibaraki 305-8571, Japan
[c] International Research Center for Elements Science, Institute for Chemical Research, Kyoto University, Gokasyo, Uji, Kyoto 611-0011, Japan

ARTICLE INFO

Article history:
Received 26 April 2014
In final form 11 May 2014
Available online 15 May 2014

ABSTRACT

A series of two-dimensional (2D) arrays of Au-core/Ag-shell nanoparticles with fixed sub-3 nm gap distance was obtained on 1 cm^2 substrates. All 2D arrays resulted in homogeneous and dense monolayers of nanoparticles thanks to our original hybrid deposition method based on self-assembly. Midnanosized gold nanoparticles were used as the core and Ag-shell with different thicknesses were grown to tune the LSPR to around 633 nm. The resulting SERS substrates enhanced Raman signal by up to about 10^7 with remarkable spatial uniformity. Our SERS substrate is highly promising as a practical SERS-based sensor substrate.

1. Introduction

Surface enhanced Raman scattering (SERS) has long been considered a promising technique for sensing applications [1–3], enabling multiplexing [4], recognition of structural properties [5] and structural changes of the analytes [6], and high lateral spatial resolution [7]. However, the potential of SERS has not materialized [8] due to limitations in the fabrication of plasmonic substrates and the lack of understanding of their near-field properties. Despite many papers on the topic [9], research on SERS has focused on maximizing the sensitivity [10,11] rather than addressing the issues of homogeneity, reliability and reproducibility of the enhancement, which are crucial for the application of SERS for quantitative analysis. Although some recent reports have focused on these issues [12–17], reflecting the importance of creating large-area homogeneous and efficient substrates for sensing applications, the respective methods have limitations such as fabrication method or limited enhancement. While a few groups succeeded in fabricating highly uniform SERS substrates, they relied on top-down methods to produce a controlled pattern [12,13], or used special vacuum setups for depositing metal nanostructures [16]; such substrates are too costly or the fabrication process is too complex. When simple wet-chemical processes were used instead, the enhancement was only moderate ($\sim 10^4$) [15] or unquantified [17], or the method was not versatile (24 nm Ag nanoclusters arrays with gap $\geqslant$ 8 nm) [14]. In addition to fabrication issues, careful characterization of the near-field response of the plasmonic substrate is needed when developing a SERS-based sensor targeting a special molecule, in order to maximize the SERS enhancement and therefore the sensitivity.

It has recently been shown that characterization of the far-field properties alone cannot fully characterize the near-field optical properties of structures that present strong coupling, e.g. nanoantennas [18,19] or aggregated nanoparticles with extremely small gap distance able to induce 'hot spots' (areas of large near-field enhancement) [20,21]. In order to solve these limitations in fabrication and careful characterization of the optical response, it is necessary to develop a two-dimensional (2D) array with homogeneous particle coverage and controlled sub-10 nm gap distance, and to carefully characterize, both experimentally and numerically, the optical response of the plasmonic substrate. We have therefore developed a hybrid deposition method, which is a self-assembly based bottom-up deposition method [22] that can deposit any kind of metallic nanoparticle (MNP) on a large (cm^2 scale) conducting substrate and results in a high MNP coverage, MNP mechanical stability and fixed gap distance. The uniformity and high nanogap density achieved by this method extend to the whole substrate (cm^2 scale) and not just a small (μm^2) region, thus giving high enhancement with remarkable uniformity, unlike most reports on bottom-up deposition methods where either uniformity or high

* Corresponding authors at: Polymer Materials Unit, National Institute for Materials Science, 1-1 Namiki, Tsukuba, Ibaraki 305-0044, Japan. Fax: +81 29 860 4718.

E-mail addresses: pincella@mailaps.org (F. Pincella), MIKI.kazushi@nims.go.jp (Kazushi Miki).

http://dx.doi.org/10.1016/j.cplett.2014.05.020
0009-2614/

enhancement is sacrificed [13,15]. We used our method to deposit gold nanoparticles (AuNPs) and gold core–silver shell Au@Ag NPs, which are particularly interesting for their tunable optical response and good shape and size control [23–27].

It was recently proven that a charge transfer complex at the interface between gold and silver can partially protect the silver shell from oxidation [28]. In addition, there has been much debate since the paper of Freeman et al. [27] on the effect of the Au@Ag core–shell structure on the intensity of the near-field enhancement. Various reports on the behavior of Au@Ag core–shell nanoparticles have described a silver-like enhancement [24], an intermediate response between Au and Ag [29], and even a decrease of the SERS signal for large Ag thickness [25,27]. Therefore, homogeneous and large-scale 2D arrays of Au@Ag NPs with controlled gap distance would be useful for investigating the contribution of the Ag shell to the near-field enhancement.

In the present study, we successfully deposited a dense 2D array of Au@Ag NPs with sub-3 nm gap distance, good NPs size distribution and tunable optical properties. Using the high-quality array, we experimentally investigated the optical properties of strongly coupled assemblies of complex MNPs. The Au@Ag NPs were synthesized with a relatively large Au-core (20 and 40 nm diameter), in consideration of a recent report [30] on the optimal size range for high near-field enhancement with isolated gold nanoparticles. The high enhancement induced by midnanosized gold nanoparticles compared to small (diameter < 20 nm) and large nanoparticles (diameter > 80 nm) was found to result from the combination of finite size effects such as surface damping of electrons, radiative damping and retardation effect. Furthermore, various Ag-shell thicknesses (alternatively referred to as 'silver content' in this article) were deposited on the gold core to achieve two important goals: tuning the LSPR around the excitation and emission wavelengths (633–700 nm) and increasing the near-field enhancement by employing a metal (Ag) with smaller plasmon damping in the visible range. The SERS substrates were shown to generate SERS enhancement of up to about 10^7 with a remarkably small standard deviation below 25% on a cm^2 scale, making them excellent candidates for SERS substrates. Finally, near-field simulations performed with discrete-dipole approximation (DDA) helped to clarify the SERS results and the effects of both size and silver content in strongly coupled nanoparticles systems such as our 2D arrays, demonstrating that far-field spectra alone are not sufficient for understanding the optical response of the 2D array.

2. Experimental

Au@Ag NPs with different Ag:Au molar ratio (see Table S1) were prepared according to the literature [28,31] (see Supporting Information), capped with mixed alkanethiols (hexanethiols:dodecanethiols = 3:1), and arrayed on a thiol-terminated ITO/quartz substrate by the hybrid deposition method [32]. This method combines electrophoretic deposition, solvent evaporation and self-assembly to form a dense monolayer of MNPs, which is strongly bound to the substrate. Briefly, MNPs redispersed in 2 mL of hexane–acetone (4:1 vol) were added in an open vessel where a voltage (1.1 V) was applied between the thiol-terminated ITO substrate (cathode) and plastic carbon (anode) electrodes placed 1.2 mm apart from each other. After solvent evaporation, the sample was annealed at 50 °C for 12 h to enable chemisorption (Au–S or Ag–S bond) of MNPs on the functionalized ITO substrates. Finally, the sample was sonicated in hexane for 30 s to remove MNPs physisorbed on the chemisorbed monolayer.

In order to calculate the enhancement factor, SERS substrate enhancement factor (SSEF) was used [33], which is a spatial- and allowed-orientation-averaged single molecule enhancement factor. This formulation of the enhancement factor is particularly suitable for comparing various 2D arrays, since it takes into account the difference in substrate coverage and in the available surface area of metallic nanoparticles. A common Raman tag [34], Rhodamine 6G (R6G), was used to characterize the SERS activity of the various substrates prepared for this letter. In order to control the amount of R6G deposited on the 2D array of MNPs, the Raman tag was vacuum-sublimated on the array to obtain a surface density of R6G of 8.2×10^{13} molecules/cm^2, corresponding to about 0.3 monolayers [35,36] (see Supporting Information for details of the R6G deposition method and estimation of R6G surface density). The normal Raman signal of a 100 mM R6G solution in water was used as the non-SERS Raman signal (see Supporting Information for details of the calculation of enhancement factor). DDA simulation of isolated MNPs (AuNPs and concentric Au@Ag NPs) surrounded by water and of trimers of the corresponding MNPs embedded in a non-absorbing dielectric medium were performed with DDSCAT 7.3 [37–39] using the filter-coupled dipole method [40,41]. The triangular trimer was chosen since it is a simple and computationally-light model containing a hot spot, and therefore can help qualitatively understand the response of our samples and the dependence on various parameters, such as size and composition (see Supporting Information for further discussion on the trimer model). In addition, the triangular trimer was preferred over the dimer model to account more easily for the polarization averaged response. The calculation volume including NP(s) was discretized by an interdipole spacing of 0.5 nm. The distance between adjacent particles was set to 3.0 nm for all calculations of NPs assemblies. Values reported by Johnson and Christy [42] were used for the refractive indices of gold and silver. Refractive index values of water reported by Hale and Querry [43] were used for the metallic NPs in aqueous solution, while the refractive index of the surrounding medium was set to 1.45 in the case of MNPs on a substrate to take into account the optical constants of both substrate and alkanethiols. The parameters (core and final radius of MNP) relative to all MNP models employed throughout this letter are listed in Table S2.

3. Results and discussion

First, morphological and optical characterizations of isolated MNPs were performed by SEM, TEM and EDX to verify the shape, size distribution and silver shell deposition (Figures 1, S1–9, and Table S3). The results showed that MNPs are mainly spherical, with a small number of nanorods produced only for 40Au@Ag NPs (40 nm Au core) with thick silver shells, and possess a sharp size distribution, with the standard deviation of MNPs' diameter not larger than 14% of the average diameter. In addition, from EDX maps and HRTEM micrographs (see Figures 1c, d, S1–4c, d, S6–9c, d), the Ag shell grows as an almost uniform layer around the Au core, although it is not perfectly concentric at large Ag shell thicknesses. The extinction spectra of colloidal solutions (Figures S10, 11) were also compared with the simulated extinction spectra obtained from DDA simulations to validate the numerical results, showing good agreement. Next, MNPs were arrayed on a conductive substrate and the formation of a dense 2D array of MNPs was verified by SEM, as shown in Figures S1–9b. The MNP coverage was estimated from SEM micrographs (from various points on the sample); the results are summarized in Table S3. The gap distance for similar 2D arrays of alkanethiol-capped MNPs on ITO substrate was previously determined by SEM and small-angle X-ray scattering measurements to be 2.4 nm due to alkyl chain interdigitation [22].

Figure 2a, c shows the extinction spectra of various 2D arrays obtained by ensemble UV–Vis spectroscopy. Note that the LSPR

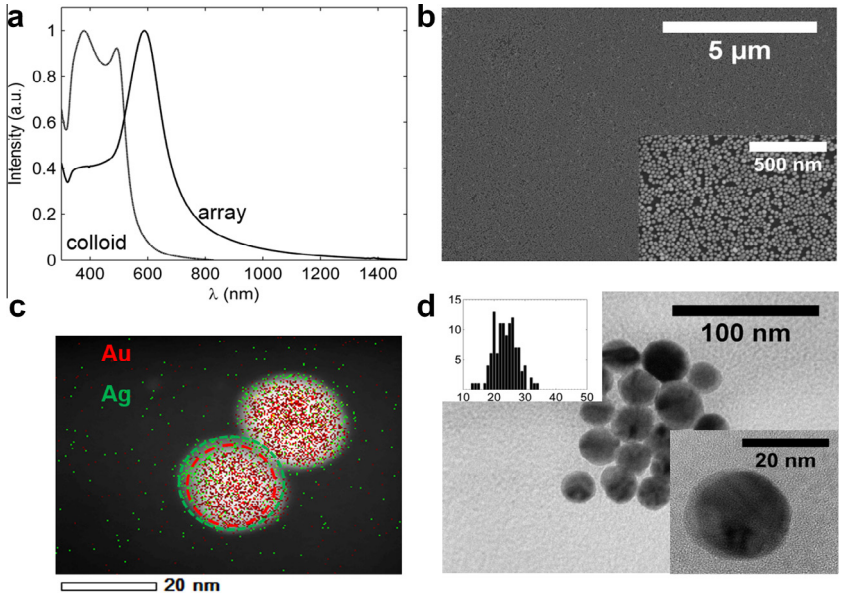

Figure 1. (a) Extinction spectra of colloidal and arrayed 20Au@$Ag_{0.7}$ NPs, (b) SEM micrograph of 2D array of 20Au@$Ag_{0.7}$ NPs (inset: higher magnification), (c) EDX map of 20Au@$Ag_{0.7}$ NPs and (d) TEM micrograph of 20Au@$Ag_{0.7}$ NPs (top inset: histogram of size distribution of 20Au@$Ag_{0.7}$ NPs, average $d = 25 \pm 3.5$ nm, bottom inset: HRTEM micrograph of 20Au@$Ag_{0.7}$ NP).

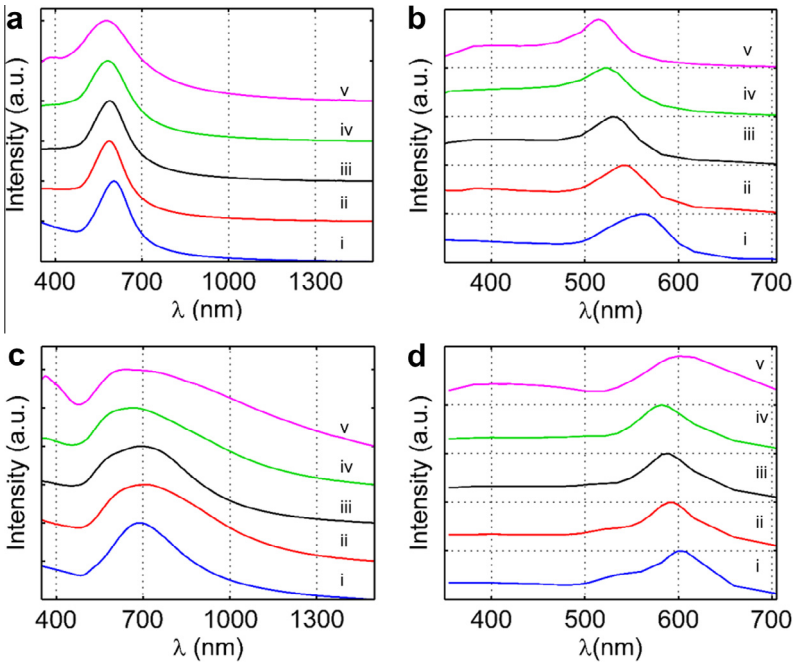

Figure 2. Comparison of experimental and simulated extinction spectra of Au@Ag NPs 2D arrays. (a) Experimental and (b) simulated extinction spectra of (i) 20AuNPs, (ii) 20Au@$Ag_{0.4}$ NPs, (iii) 20Au@$Ag_{0.7}$ NPs, (iv) 20Au@Ag_1 NPs, (v) 20Au@Ag_3 NPs. (c) Experimental and (d) simulated extinction spectra of (i) 40AuNPs, (ii) 40Au@$Ag_{0.4}$ NPs, (iii) 40Au@$Ag_{0.7}$ NPs, (iv) 40Au@Ag_1 NPs, (v) 40Au@Ag_3 NPs. Each spectrum is normalized to its maximum value and vertically shifted for clarity. Note that the abscissa in (a) and (c) is different from that in (b) and (c).

peak is remarkably sharp due to the good size distribution of the MNPs and their controlled gap distance, compared to previous reports on arrays of AuNPs and silver nanoparticles (AgNPs) prepared by self-assembly methods [44]. This peak shows a gradual blueshift with the silver content, from the starting core NP (LSPR = 603 nm for 20 nm AuNPs, LSPR = 688 nm for 40 nm AuNPs) to the Au@Ag with the Ag:Au molar ratio of 3:1 (LSPR = 577 nm for 20Au@Ag_3, LSPR = 635 nm for 40Au@Ag_3), for both 20Au@Ag NPs and 40Au@Ag NPs, although in the latter case the LSPR peaks are broader and seem to contain two overlapping contributions in the case of core–shell 2D arrays, probably due to an almost overlapping higher order mode. Experimental extinction spectra of 2D arrays were then compared with the simulated spectra of corresponding trimers. As can be seen from Figure 2b, d, the simulated spectra show a similar tendency but do not completely agree with the experimental data regarding the LSPR position. The discrepancies between simulations and experimental results are clearly due to the limitations of the model used for this simulation. For example, our calculations do not take several effects into account, such as the size distribution, non-perfect concentricity of the NPs, larger

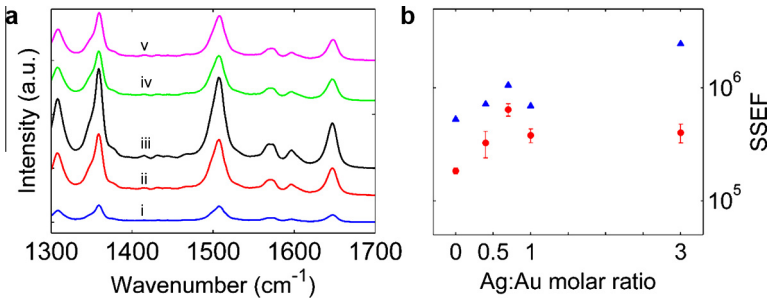

Figure 3. (a) SERS spectra of R6G deposited on (i) 20AuNPs, (ii) 20Au@$Ag_{0.4}$ NPs, (iii) 20Au@$Ag_{0.7}$ NPs, (iv) 20Au@Ag_1 NPs, and (v) 20Au@Ag_3 NPs 2D arrays. All SERS spectra are vertically shifted by a constant value for clarity. (b) Comparison of experimental SSEF obtained from SERS spectra of R6G on 20Au@Ag NPs arrays (circles) and corresponding simulated EF for 20Au@Ag NPs trimers (triangles).

extent of the coupling (not limited to an isolated trimer), and the broken symmetry induced by the substrate. These effects, together with the slightly larger gap distance used for the simulations (3 nm instead of 2.4 nm), account for the difference between the LSPR wavelength in the simulated and experimental data (around 50 nm blueshift in DDA results), since strong coupling and narrower gap distance are expected to induce a redshift of the LSPR [45].

After checking the far-field optical properties of various 2D arrays, these samples were employed as SERS substrates. The SERS spectra of R6G deposited on 20AuNPs and 20Au@Ag NPs 2D arrays are shown in Figure 3a (only one spectrum for each plasmonic substrate is shown for clarity). In Figure 3b the experimental SSEFs and their standard deviation (error bar in the plot) are shown; each experimental value in Figure 3b was obtained from the average of six different points in the corresponding substrate. Figure 3b reveals a peculiar tendency of the SSEF: at first SSEF increases up to 20Au@$Ag_{0.7}$, drops at 20Au@Ag_1, then increases slightly for 20Au@Ag_3. The maximum value of SSEF in a determined position was obtained for the 20Au@$Ag_{0.7}$ 2D array and corresponds to 7.9×10^5, while the average SSEF over six points of the same substrate gives an SSEF of 6.4×10^5. The experimental SSEFs are found to be extremely uniform over the whole substrate with the largest standard deviation being 25% of the relative SSEF value. To confirm the homogeneous response over the sample, Raman intensity maps were also acquired for some test 2D array substrates (an example map is shown in Figure 4a) and compared to a sparse sub-monolayer of AuNPs (Figure 4b for the Raman map and Figure S13 for the SEM micrograph) obtained by self-assembly (details in Supporting Information) [44,46]. Comparing Figure 4a and b, our 2D array shows a uniform intensity over the whole area, while the sparse sub-monolayer shows an inhomogeneous response with local 'hot spots', corresponding probably to dimers or small aggregates, similar to the result obtained in [44] in the case of a sparse MNP monolayer. This result confirms that our array provides a uniform SERS signal while maintaining high enhancement, unlike previously reported nanoparticle cluster arrays [13] or Ag nanowire arrays [15] where the highest enhancement was five times or one order of magnitude lower, respectively. This finding is of great importance for the development of SERS substrates with controllable enhancement over the whole area (not dependent on localized 'hot spots'), which is a key issue for the development of SERS-based sensors.

After analysis of experimental data, the experimental values of enhancement factor (SSEFs) were compared with those obtained from simulations (EF, details in Supporting Information). Figure 3b shows very good agreement between the SSEF and the EF, although the SSEF values are constantly overestimated by the simulation. The difference between simulated and experimental values is due to the fact that the experimental enhancement factor is by definition an average value, with contributions coming from both hot spots and areas with low or no enhancement, while the simulated enhancement factor corresponds to the maximum enhancement at the hot spot.

From Figure 3b, it is clear that the tendency of the SSEF cannot be explained simply as a function of the silver content or the LSPR matching: SSEF does not monotonically change with the Ag content in the particles or with the distance between the LSPR and the excitation wavelength. Since the far-field response alone was not enough to clarify the origin of this tendency, the simulated near-field spectra of Au@Ag NPs trimers were analyzed. Near-field spectra were obtained by plotting the maximum value of the near-field intensity enhancement outside the nanostructures ($\mathrm{Max}(|E|^2/|E_o|^2)$, where E_o is the incident electric field) for various excitation wavelengths (from 300 to 600 nm, in steps of 10 nm, except near LSPR where sampling was increased). First, taking into account the comparison of experimental and simulated extinction spectra, the excitation light (633 nm laser) is resonant with the long wavelength mode in the experimental extinction spectra, which corresponds to the 500–560 nm mode in the simulated spectra. From a comparison of the far-field spectra in Figure 2b, d and the near-field spectra in Figure 5a and S14a (20 nm and 40 nm series, respectively), the long wavelength mode in the near-field spectra (dotted line) is found to be redshifted by about 20 nm compared to the same mode in the simulated extinction spectra [47–49].

From the near-field spectra in Figure 5a, the deposition of a thin Ag shell (20Au@$Ag_{0.4}$ and 20Au@$Ag_{0.7}$ trimers) induces a gradual increase of the near-field enhancement. Furthermore, the wavelength corresponding to the maximum near-field enhancement is found to blueshift with increasing Ag content, as shown in Figure 5b. In the case of 20Au@Ag_1 trimer both these tendencies are inverted: the enhancement is found to decrease slightly compared to 20Au@$Ag_{0.7}$, and the wavelength corresponding to the maximum enhancement is redshifted by about 15 nm compared to the peak value for 20Au@$Ag_{0.7}$. This phenomenon can be explained heuristically by the transition from a 'core-like' behavior that is dominant only for very thin silver shells, where the dipoles of the gold core and the dipoles of the silver shell respond in phase to the incident electric field, to a 'shell-like' behavior, where the dipoles in the core and those in the shell respond out of phase. As can be deduced from both experimental results and simulations, this transition occurs at an Ag:Au molar ratio of approximately one. Near the transition point the contribution of the silver shell is expected to partially screen the contribution of the gold core (subradiant mode), inducing a decrease in the net dipole of the core–shell and a consequent decrease in the near-field enhancement. Interestingly, the same inversion of tendency (from increase to decrease in enhancement) was found also for randomly-aggregated Au@Ag NPs in solution [25], confirming that this behavior is linked to the optical response of the core–shell particles

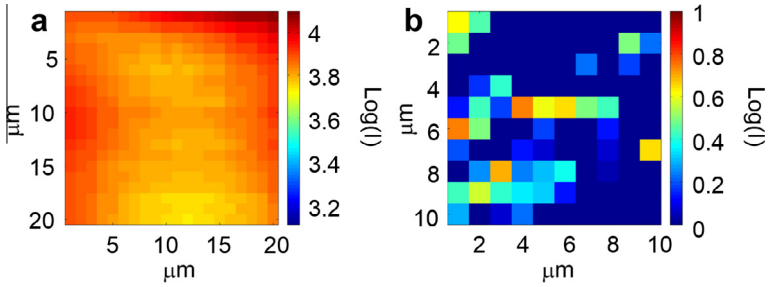

Figure 4. (a) Raman intensity map obtained from 20Au@$Ag_{0.7}$ 2D array with 1 μm step, 45 × objective, and 1 s accumulation. The logarithm of intensity of the 1510 cm^{-1} peak of R6G was analyzed after baseline subtraction. The standard deviation in intensity over the whole 20 × 20 $μm^2$ area corresponds to 15% of the average value of the intensity. (b) Raman intensity map obtained from a sparse monolayer of 40AuNPs with 1 μm step, 45 × objective, and 10 s accumulation. R6G was vacuum-sublimated following the same procedure used for the 2D arrays in order to achieve the same dye density. The logarithm of intensity of the 1510 cm^{-1} peak of R6G was reported after baseline subtraction and division by total accumulation time. The standard deviation in intensity over the whole 10 × 10 $μm^2$ area corresponds to 93% of the average value of the intensity. The map clearly shows the presence of hot spots due to local high enhancement occurring probably near AuNPs dimers or small aggregates together with a large area with no intensity coming from completely uncoated regions or regions with isolated AuNPs, as shown in Figure S13 (note that the area of the map does not correspond exactly to the area shown in the SEM micrograph, therefore correlation cannot be made).

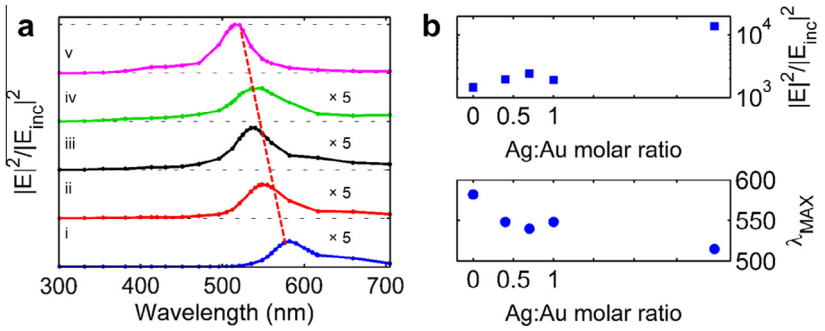

Figure 5. (a) Comparison of near-field intensity enhancement spectra (averaged over two perpendicular polarizations) for the 20Au@Ag series. The spectra are normalized to the maximum enhancement of the whole series (value relative to 20Au@Ag_3). From the bottom: near-field enhancement spectrum of trimer of (i) 20AuNPs, (ii) 20Au@$Ag_{0.4}$ NPs, (iii) 20Au@$Ag_{0.7}$ NPs, (iv) 20Au@Ag_1 NPs, and (v) 20Au@Ag_3 NPs. Spectra from (i) to (iv) are multiplied by a factor of 5 and all spectra are vertically shifted by a constant value for clarity. (b) Top: maximum of simulated near-field intensity enhancement vs. Ag:Au ratio, bottom: dependence of wavelength position relative to maximum enhancement on Ag:Au molar ratio. The dotted line (guide for the eye) indicates roughly the position of the LSPR peak corresponding to the long wavelength mode in the far-field spectrum.

and not to this particular ordered structure. For larger shells, instead, the 'shell-like' behavior becomes dominant and the net dipole of the core–shell increases again together with the near-field enhancement, as confirmed experimentally.

An analogous characterization was performed for the 40 nm core series (see Figure 6). The maximum SSEF achieved for the 40Au@Ag_3 at one point is 7.5×10^6, comparable with reports on self-assembled films of silver nanoparticles [44], while the average SSEF over six points in the same sample gives a value of 5.9×10^6, one order of magnitude bigger than that for 20Au@Ag NPs arrays. This result may be related to the size effect [30], and good matching of LSPR with excitation and emission wavelengths, since the broad LSPR peak is resonant with both laser excitation and Raman scattered light. The effect of the silver shell can also be observed by comparing 2D arrays of metallic nanoparticles of similar final size and different metallic composition: the 40AuNPs 2D array (average diameter = 38 nm) gives an average enhancement of 6.2×10^4, while the core–shell 20Au@Ag_3 2D array (average diameter = 34 nm) gives a 6.5 times higher average enhancement (4.0×10^5), showing that the contribution of silver to SERS enhancement is larger than that of gold even for excitation in the red region of the spectrum (633 nm), where losses in silver start to become relevant.

Figure 6b reveals good agreement between the simulated EFs obtained from the near-field spectra in Figure S14a and the experimental SSEFs for 40Au@Ag NPs, with the simulated values being

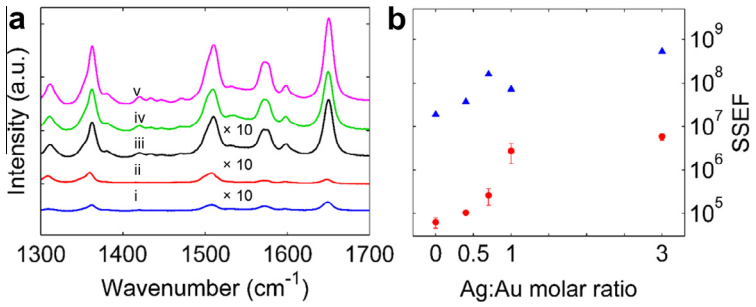

Figure 6. (a) SERS spectra of R6G deposited on (i) 40AuNPs, (ii) 40Au@$Ag_{0.4}$ NPs, (iii) 40Au@$Ag_{0.7}$ NPs, (iv) 40Au@Ag_1 NPs, and (v) 40Au@Ag_3 NPs 2D arrays. Spectra from (i) to (iii) are multiplied by a factor of 10 and all SERS spectra are vertically shifted by a constant value for clarity. (b) Comparison of experimental SSEF obtained from SERS spectra of R6G on 40Au@Ag NPs arrays (circles), corresponding simulated EF for 40Au@Ag NPs trimers (triangles). Simulated value of 40Au@Ag_1 NPs trimer (triangle) overlaps with the experimental value.

more than an order of magnitude higher than the experimental ones, probably due to the poor close-packing of the 2D array of large MNPs and the consequent larger gap distance between MNPs (compared to the value chosen for simulations), which negatively affects enhancement [45]. In the case of 40Au@Ag NPs arrays, no decrease of the enhancement factor for Ag:Au around 1 was observed experimentally, different from the simulated results shown in Figure 6b. This phenomenon may be due to the fact that large 40Au@Ag NPs have broad size distributions and imperfect shapes (non-concentric and non-spherical) that do not allow observation of the 'transition point' around Ag:Au equal to 1 and the consequent inversion of the tendency.

4. Conclusions

In conclusion, promising plasmonic arrays of Au@Ag NPs were obtained by our original hybrid deposition method [22], which is a bottom-up deposition method based on self-assembly. This method was proven to provide cm^2 scale arrays with high coverage, fixed gap distance (below 3 nm), and strong mechanical stability. The method is also very versatile and allows the array properties to be customized, since particles of various sizes and compositions can be effectively arrayed. These arrays were characterized experimentally by UV–Vis spectroscopy and SERS, and their optical response was also studied computationally, revealing their potential as efficient SERS substrates in the visible range. The highest average enhancement factor, 5.9×10^6 was achieved for the 2D array of 40Au@Ag_3 NPs that are 40 nm core particles with Ag to Au molar ratio of three. Up to this value of the Ag to Au ratio, MNPs were produced with a sharp size distribution, which is suitable to achieve dense arrays with optimal control of optical properties. For larger Ag to Au molar ratio, we found that the shell did not grow uniformly around the core, but easily gave rise to nanorods or particles of different shapes and final sizes. The SERS enhancement factor was also proven to be homogeneous over the substrate, with the highest relative standard deviation of the enhancement factor being 25% over a cm^2 scale. These results indicate that this self-assembled 2D array is a reliable SERS substrate candidate for the development of practical SERS-based sensors. In addition, it was found that the near-field response of the 2D array cannot be straightforwardly predicted by studying its far-field response, since the latter cannot account both for the exact position (red-shift) and for the intensity of the maximum enhancement.

Acknowledgements

We thank the Japan Society for the Promotion of Science (JSPS) and the Ministry of Education, Culture, Sports, Science and Technology of Japan (MEXT) for financial support; Grant-in-Aid for Challenging Exploratory Research (K.M., 24656040); Grant-in-Aid for Scientific Research on Innovative Areas "Integrated Organic Synthesis" (K.M., 22106545 & 24106746); and Grant-in-Aid for Young Scientists (K.I., 30455274), Japan Science and Technology Agency (JST) for financial support of e-ASIA JRP. Also, a part of this research was supported by the Yazaki Memorial Foundation for Science and Technology. This study was supported by NIMS Molecule & Material Synthesis Platform in the "Nanotechnology Platform Project" operated by the Ministry of Education, Culture, Sports, Science and Technology (MEXT), Japan. We thank Prof. H.T. Miyazaki for helpful discussions.

Appendix A. Supplementary data

Supplementary data associated with this article can be found, in the online version, at http://dx.doi.org/10.1016/j.cplett.2014.05.020.

References

[1] M. Moskovits, Rev. Mod. Phys. 57 (1985) 783.
[2] K. Kneipp et al., Phys. Rev. Lett. 78 (1997) 1667.
[3] K. Kneipp, H. Kneipp, I. Itzkan, R.R. Dasari, M.S. Feld, J. Phys. Condens. Matter. 14 (2002) R597.
[4] T. Kang, S.M. Yoo, I. Yoon, S.Y. Lee, B. Kim, Nano Lett. 10 (2010) 1189.
[5] P. Leyton et al., J. Phys. Chem. B 108 (2004) 17484.
[6] T.-T. Liu et al., PLoS ONE 4 (2009) e5470.
[7] R. Stöckle, Y. Suh, V. Deckert, R. Zenobi, Chem. Phys. Lett. 318 (2000) 131.
[8] M.J. Natan, Faraday Discuss. 132 (2006) 321.
[9] M. Pelton, J. Aizpurua, G. Bryant, Laser Photonics Rev. 2 (2008) 136.
[10] J. Lee, J. Nam, K. Jeon, D. Lim, H. Kim, ACS Nano 6 (2012) 9574.
[11] S. Nie, S.R. Emory, Science 275 (1997) 1102.
[12] K.D. Alexander, M.J. Hampton, S. Zhang, A. Dhawan, H. Xu, R. Lopez, J. Raman Spectrosc. 40 (2009) 2171.
[13] B. Yan, A. Thubagere, W.R. Premasiri, L.D. Ziegler, L. Dal Negro, B.M. Reinhard, ACS Nano 3 (2009) 1190.
[14] W.J. Cho, Y. Kim, J.K. Kim, ACS Nano 6 (2012) 249.
[15] M. Chen, I.Y. Phang, M.R. Lee, J.K.W. Yang, X.Y. Ling, Langmuir 29 (2013) 7061.
[16] N.G. Greeneltch, M.G. Blaber, A.-I. Henry, G.C. Schatz, R.P. Van Duyne, Anal. Chem. 85 (2013) 2297.
[17] N. Pazos-Pérez, W. Ni, A. Schweikart, R.A. Alvarez-Puebla, A. Fery, L.M. Liz-Marzán, Chem. Sci. 1 (2010) 174.
[18] S.L. Kleinman et al., J. Am. Chem. Soc. 135 (2013) 301.
[19] K.L. Wustholz et al., J. Am. Chem. Soc. 132 (2010) 10903.
[20] J. Litz, J. Camden, D. Masiello, J. Phys. Chem. Lett. 2 (2011) 1695.
[21] L.K. Ausman, G.C. Schatz, J. Chem. Phys. 131 (2009) 084708.
[22] K. Isozaki, T. Ochiai, T. Taguchi, K. Nittoh, K. Miki, Appl. Phys. Lett. 97 (2010) 221101.
[23] L. Liz-Marzán, Langmuir 22 (2006) 32.
[24] L. Lu et al., Chem. Commun. (Camb) (2002) 144.
[25] N.R. Jana, Analyst 128 (2003) 954.
[26] P.R. Selvakannan et al., Langmuir 20 (2004) 7825.
[27] R.G. Freeman, M.B. Hommer, K.C. Grabar, M.A. Jackson, M.J. Natan, J. Phys. Chem. 100 (1996) 718.
[28] C. Shankar, A. Dao, P. Singh, K. Higashimine, F.M. Mott, S. Maenosono, Nanotechnology 23 (2012) 245704.
[29] L. Rivas, S. Sanchez-Cortes, J.V. Garcia-Ramos, G. Morcillo, Langmuir 16 (2000) 9722.
[30] C. Deeb, X. Zhou, J. Plain, J. Phys. Chem. C 117 (2013) 10669.
[31] Y.-K. Park, S. Park, Chem. Mater. 20 (2008) 2388.
[32] T. Ochiai, K. Isozaki, F. Pincella, T. Taguchi, K. Nittoh, K. Miki, Appl. Phys. Express 6 (2013) 102001.
[33] E.C. Le Ru, E. Blackie, M. Meyer, P.G. Etchegoin, J. Phys. Chem. C 111 (2007) 13794.
[34] A.M. Michaels, L. Brus, J. Phys. Chem. B 104 (2000) 11965.
[35] M.D. Elking, G. He, Z. Xu, J. Chem. Phys. 105 (1996) 6565.
[36] A. Kudelski, Chem. Phys. Lett. 414 (2005) 271.
[37] B.T. Draine, P.J. Flatau, J. Opt. Soc. Am. A 11 (1994) 1491.
[38] B.T. Draine, P.J. Flatau, J. Opt. Soc. Am. A. Opt. Image Sci. Vis. 25 (2008) 2693.
[39] P.J. Flatau, B.T. Draine, Opt. Express 20 (2012) 1247.
[40] M.A. Yurkin, M. Min, A.G. Hoekstra, Phys. Rev. E 82 (2010) 036703.
[41] N. Piller, O. Martin, IEEE Trans. Antennas Propag. 46 (1998) 1126.
[42] P. Johnson, R. Christy, Phys. Rev. B 6 (1972) 4370.
[43] G.M. Hale, M.R. Querry, Appl. Opt. 12 (1973) 555.
[44] V. Joseph, M. Gensler, S. Seifert, U. Gernert, J.P. Rabe, J. Kneipp, J. Phys. Chem. C 116 (2012) 6859.
[45] P.K. Jain, W. Huang, M.A. El-Sayed, Nano Lett. 7 (2007) 2080.
[46] H. Zhu, L. Bao, S.M. Mahurin, G.A. Baker, E.W. Hagaman, S. Dai, J. Mater. Chem. 18 (2008) 1079.
[47] J. Zuloaga, P. Nordlander, Nano Lett. 11 (2011) 1280.
[48] R. Marty, G. Baffou, A. Arbouet, C. Girard, R. Quidant, Opt. Express 18 (2010) 3035.
[49] S. Bruzzone, M. Malvaldi, J. Phys. Chem. B 110 (2006) 11050.